GA–A23398

THE EFFECT OF DIVERTOR MAGNETIC BALANCE ON H–MODE PERFORMANCE IN DIII–D

by
T.W. PETRIE, S.L. ALLEN, M.E. FENSTERMACHER,
R.J. GROEBNER, A.W. HYATT, R.J. LA HAYE, A.W. LEONARD,
M.A. MAHDAVI, T.H. OSBORNE, C.J. LASNIER, G.D. PORTER,
T.L. RHODES, M.J. SCHAFFER, D.M. THOMAS, J.G. WATKINS,
W.P. WEST, and the DIII–D TEAM

JULY 2000

DISCLAIMER

GA–A23398

THE EFFECT OF DIVERTOR MAGNETIC BALANCE ON H–MODE PERFORMANCE IN DIII–D

by
T.W. PETRIE, S.L. ALLEN,[*] M.E. FENSTERMACHER,[*]
R.J. GROEBNER, A.W. HYATT, R.J. LA HAYE, A.W. LEONARD,
M.A. MAHDAVI, T.H. OSBORNE, C.J. LASNIER,[*] G.D. PORTER,[*]
T.L. RHODES,[†] M.J. SCHAFFER, D.M. THOMAS, J.G. WATKINS,[‡]
W.P. WEST, N.S. WOLF,[*] and the DIII–D TEAM

This is a preprint of a paper presented at the 14th International Conf. on Plasma Surface Interactions in Controlled Fusion Devices, May 22–26, 2000 in Rosenheim, Germany and to be published in *J. Nucl. Mater.*

[*]Lawrence Livermore National Laboratory, Livermore, California
[†]University of California, Los Angeles, California
[‡]Sandia National Laboratories, Albuquerque, New Mexico

Work supported by
the U.S. Department of Energy under Contract Nos. DE-AC03-99ER54463,
W-7405-ENG-48, DE-AC04-94AL85000, and Grant No. DE-FG03-86ER53225

GA PROJECT 30033
JULY 2000

ABSTRACT

We report on recent experiments for which the magnetic balance of highly triangular ($\delta \approx 0.8$), unpumped H–mode plasmas was varied. Changes in divertor heat loading and particle flux were observed when the magnetic configuration was varied from a balanced double-null (DN) divertor to a slightly unbalanced DN divertor. For attached plasmas, the variation in heat flux sharing between divertors is very sensitive near balanced DN. This sensitivity can be shown to be consistent with the measured scrape-off length width of the parallel divertor heat flux, $\lambda_{q_{||}}$. At magnetic balance we find that the peak heat flux toward the divertor in the ∇B ion drift direction is twice that of the other divertor. Most of the heat flux goes to the outboard divertor targets in a balanced double-null, where the peak heat flux at the outer divertor targets may exceed that of the inner divertor targets by tenfold. However, the variation of the peak particle flux between divertors is less sensitive to changes in magnetic balance. These particle and heat flux "asymmetries" in DN plasmas are consistent with the presence of $E \times B$ poloidal particle drifts in the scrape-off layer and private flux region [1]. Regardless of how the divertors were magnetically balanced, D_2 gas puffing always reduced energy confinement to the range $\tau_E/\tau_{E89P} \approx 1.3–1.6$. When this energy confnement range was reached, τ_E/τ_{E89P} remained nearly constant up to near the H–mode density limit.

1. INTRODUCTION

Plasma performance in tokamaks generally improves with increased shaping of the plasma cross section. This stronger shaping, especially higher triangularity, can produce changes in the magnetic topology of the divertor. Important engineering and divertor physics issues (e.g., power flow handling) are associated with changes in the details of the divertor geometry, especially as the configuration transitions from a single-null (SN) divertor to a marginally balanced double-null (DN) divertor. In this paper, we examine how variation in magnetic balance affects (1) heat flux and particle sharing by the divertors and (2) the response of the plasma confinement properties to deuterium gas fueling. To quantify the degree of “divertor imbalance” (or equivalently, to what degree the shape is “double-null” or “single-null”), we introduce a parameter *drSEP*, which we define as the radial distance between the upper divertor separatrix and the lower divertor separatrix at the outboard midplane. For example, if drSEP=0, the configuration is a magnetically balanced DN; if drSEP = +1.0 cm, the upper divertor separatrix is innermost by 1 cm at the outer midplane. Two examples are shown in Fig. 1. The experimental parameters are listed in the caption to Fig. 1.

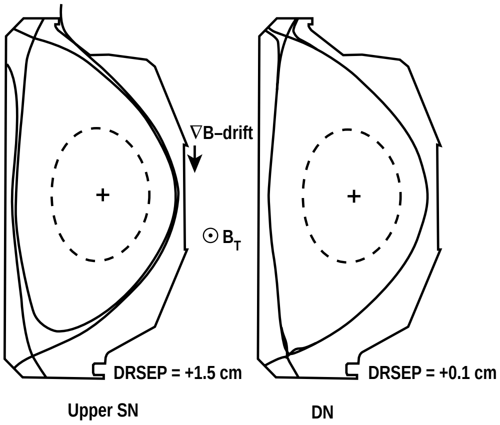

Fig. 1. Two of the plasma shapes considered in this study are shown: drSEP= +1.5 cm (upper SN) and drSEP = +0.1 cm (near-balanced DN). The direction of the toroidal field in "out of the paper" (i.e., the ∇B ion drift is toward the lower divertor). The direction of the plasma current is "into the paper." Plasma parameters: I_P = 1.37 MA, B_T = 2.0 T, q_{95} = 4–5, triangularity of the primary X–point = 0.78, P_{input} = 4.5–7.0 MW, Z_{eff} = 1.7, drSEP = –4 cm to +4 cm. No active particle pumping at the divertor strike points or in the private flux region was done for these discharges.

2. HEAT AND PARTICLE FLUXES

The peak parallel heat flux under either outboard divertor in *attached* plasmas [2] is strongly dependent on the magnetic balance between drSEP = –1 cm and + 1 cm [Fig. 2(a)]. These data (●), fitted to a hyperbolic tangent function, are not symmetric with respect to drSEP=0. At magnetic balance, the parallel peak heat flux to the lower divertor $\left(q^{p}_{\|low}\right)$ is approximately twice that of the upper divertor $\left(q^{p}_{\|up}\right)$. Up/down balance in the peak heat flux occurs for drSEP ≈0.25 cm. This “offset” is observed in detached plasmas [1] as well (o), but the slope in that curve near drSEP=0 is much less steep, also shown in Fig. 2(a). An “offset” asymmetry in the peak particle flux between upper and lower outboard (attached) divertors is shown in Fig. 2(b). Unlike the case for the heat flux asymmetry, the peak particle flux to the upper divertor is *higher* than that to the lower divertor at magnetic balance.

Most of the heat is deposited to the outboard divertor targets in a balanced DN divertor [Figs. 3(a,b)]. The ratio of the outboard-to-inboard peak heat flux $\left(q^{p}_{out}/q^{p}_{in}\right)$ in both upper and lower divertors is ≈ 2.5 over most of the range in drSEP. Near magnetic balance, however, $q^{p}_{out} >> q^{p}_{in}$ in both divertors. Our interpretation of these data will be presented in Section 5.

We have determined the scrape-off width, $\lambda_{q_\|}$, for the parallel heat flux by projecting the heat flux distribution from the divertors back to the midplane using the EFITD [3] magnetic reconstruction code and the VIDDAPS [4] heat flux analysis code, and then fitting the result to an exponential function. The results, plotted in Fig. 4, show that the scrape-off length of the parallel heat flux at the outboard midplane for attached plasmas varies between 0.4 cm and 0.6 cm. The solid circles represent $\lambda_{q_\|}$ determined by an infrared camera monitoring the lower divertor and the open circles determined by an infrared camera monitoring the upper divertor. For drSEP < 0, $\lambda_{q_\|} \approx 0.6$ cm and for drSEP > +2.0 cm, $\lambda_{q_\|} \approx 0.5$ cm; has a minimum of ≈0.4 cm for drSEP ≈ +1.0 cm. When $\lambda_{q_\|}/|\mathrm{drSEP}| << 1$, $\lambda_{q_\|}$ corresponding to the primary separatrix is

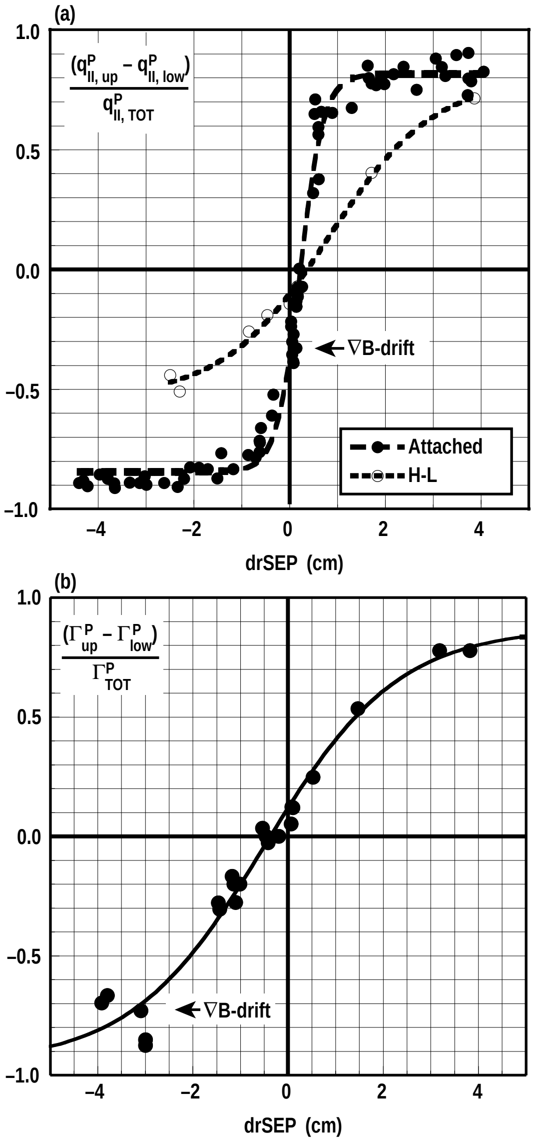

Fig. 2. (a) Peak parallel heat flux for "attached" divertors is roughly a factor of 2 higher in the “lower” divertor, when the configuration is in magnetic balance (●). The peak heat flux is balanced when drSEP ≈ 0.25 cm. To a lesser degree, asymmetries in the peak heat flux is observed in "detached" divertors (o), (b) There is also an asymmetry in the peak particle flux between the upper divertor and lower divertor. $q^{p}_{\|-\mathrm{tot}}$ and $\Gamma^{p}_{\|-\mathrm{tot}}$ are the *sum* of the upper and lower peak parallel heat flux and peak particle flux, respectively. The data are fit to a hyperbolic tangent function. Uncertainty in drSEP < 0.2 cm.

insensitive to drSEP. However, when drSEP is roughly equal to $\lambda_{q_{\|}}$, the “secondary” divertor, as expected, begins to siphon off significant power.

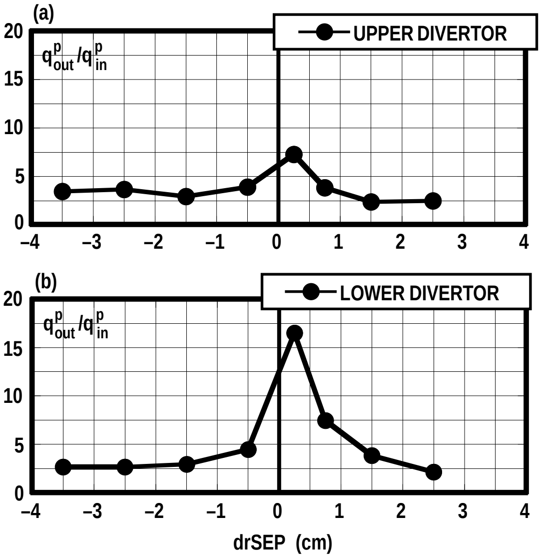

Fig. 3. The ratio of the outboard peak heat flux to the inboard peak heat flux in the (a) upper divertor and (b) lower divertor. Measurements are made with infrared cameras.

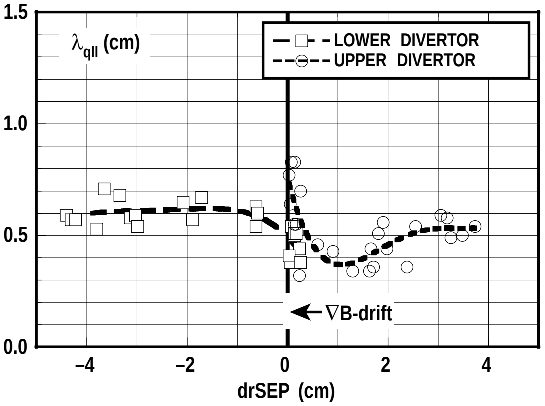

Fig. 4. The scrapeoff length ($\lambda_{q_{||}}$) of the parallel heat flux at the outboard midplane is insensitive to changes in magnetic balance, except between drSEP = 0 and 1 cm. Infrared camera data from the lower (G) and upper (E) divertor are used. Polynomial fits to each dataset are shown. The scrape-off profiles at the midplane are found by projecting the heat flux distribution from the divertors back to the midplane using the EFITD [3] magnetic reconstruction code and the VIDDAPS [4] heat flux analysis code.

3. RESPONSE TO GAS INJECTION

Gas puffing reduced the energy confinement of these ELMing H–mode discharges to levels where $\tau_E/\tau_{E89P} \approx 1.3–1.6$, *independent* of the drSEP value, where τ_{E89P} refers to the 1989 ITER-L–mode scaling [5]. When this energy confinement range was reached, τ_E/τ_{E89L} remained nearly constant during further gas puffing up to near the H-L back transition, as shown below. For these unpumped plasmas, we have not been able to fuel an ELMing H–mode plasma to high density with gas puffing only, and simultaneously maintain an energy confinement of $\tau_E/\tau_{E89P} \approx 2$.

In general, there were two distinct phases of plasma behavior during gas puffing (Fig. 5). Phase I, which covered approximately the first 0.5 s of deuterium gas puffing [Γ_{D2} = 60 Torr ℓ/s, Fig. 5(b)], was characterized by a drop in τ_E/τ_{E89P}, as well as a coincident drop in edge electron pressure $P_{e,ped}$ [Fig. 5(c)]. Neither the line-averaged density $\bar{n}_e$ nor the pedestal [6] electron density $n_{e,ped}$ increased [Fig. 5(d)]. Phase II was characterized by a "plateau" in τ_E/τ_{E89P} (≈1.4); for our data set, τ_E/τ_{E89P} lay in the range 1.3–1.6 during the "plateau" phase, irrespective of drSEP. Note also that the "edge" or pedestal electron pressure was also constant and that steady fueling of the main plasma was coincident with the start of Phase II.

Confinement degradation was not limited to the edge plasma. We examined the radial profiles in density and temperature at three timeslices for the shot shown in Fig. 5: (1) t = 3.25 s (at the start of deuterium puffing), (2) t = 3.75 s (start of Phase II), and (3) t = 5.0 s (well into the density rise during Phase II). The radial electron density profile was virtually unchanged between 3.25 s and 3.75 s; steady fueling of the core plasma occurred only during Phase II. In Phase I both electron and ion temperatures decreased ≈30% in the outer region of the main plasma ($\rho/a > 0.6$) and decreased ≈10%–25% in the interior regions. During Phase II both electron and ion temperatures continued to decrease across the radial profile, but (with the rise in electron density) the plasma pressure across the profile remained approximately constant in time.

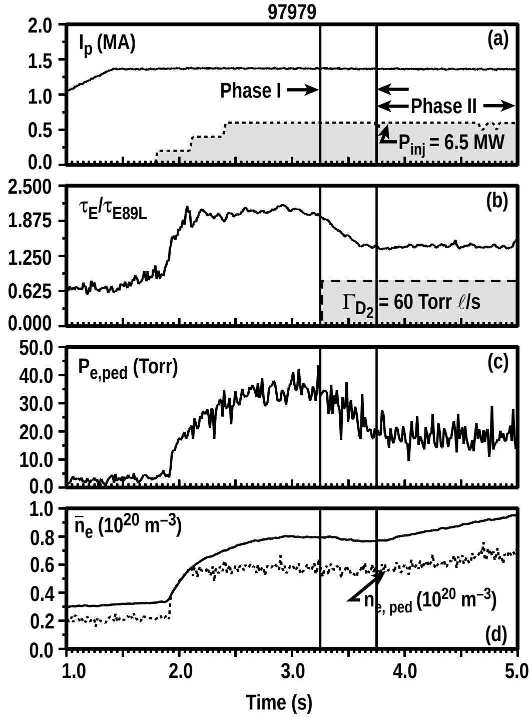

Fig. 5. Deuterium gas is injected into a lower SN divertor plasma, starting at t = 3.25 s. drSEP = –3.7 cm. Phase I: Electron energy confinement degrades with little rise in density. Phase II: Energy confinement is stable and density rises.

The initial decrease in energy confinement following the start of gas puffing may be mostly a consequence of increased ion transport, as determined from ONETWO transport code [7] analysis. This analysis also indicates that electron conductivity did not change appreciably during Phase I for $\rho < 0.7$. Ion conductivity, however, increased by about a factor of 2–4 across the entire profile during this time. While the electron conductivity inside the q = 2 flux surface was still considerably higher than the ion conductivity by the end of phase I, the ion conductivity rose to comparable values with electron conductivity outboard of the q = 2 surface. Stacey has analyzed this shot from an edge plasma stability perspective [8] and has concluded that this increase in ion conductivity (but not in electron conductivity) may be caused by short radial wavelength thermal instabilities in the ion channel, driven by radiation and atomic physics at the edge [9].

4. DISCUSSION

The observed heat and particle flux asymmetries may be driven by E×B poloidal drifts. This is suggested by experiments and modeling from SN plasmas. For example, E×B poloidal particle flow across the private flux region (PFR) were measured in DIII–D divertor plasmas and found to be in agreement with the particle flow predicted by modeling [1,10]. At present, the modeling of these symmetry-breaking particle drifts *in the DN configuration* is only at a rudimentary level for available 2-D fluid modeling edge transport codes, such as UEDGE [11]. Yet, the fact that 2-D fluid modeling (UEDGE) has been used successfully to study the importance of E×B drifts in the less complicated (SN) configurations gives confidence that our basic understanding of E×B edge plasma drifts is grounded well enough to hypothesize what these drifts might might be doing in the DNs.

Up/down asymmetries DN: The origin of the electric field (**E**) which drives the drift in the PFR arises mainly from the radial gradient in the electron temperature with respect to the flux surfaces in the PFR and its direction is always into the PFR. The direction of the toroidal field **B** is shown in Fig. 1. Thus, the direction of the **E**×**B** poloidal flow in the *lower* divertor is from the outboard leg to the inboard leg across the PFR. On the other hand, in the *upper* divertor, the direction of this flow is from the inboard divertor leg to the outboard divertor leg. In a balanced DN divertor, including these E×B drifts would lead to a higher particle flux to the upper outboard (OU) divertor target than to to the lower outboard (LO) divertor target, as seen in the experiment [Fig. 2(b)]. This asymmetry in peak particle flux implies higher particle density at the UO and lower inboard (LI) targets, as compared with the LO and upper inboard (UI) targets, respectively. In turn, this higher density, taken together with an assumption of constant plasma pressure along field lines connecting the respective upper and lower divertors, results in lower electron temperatures (T_e) and lower heat flux for LI versus UI and UO versus LO, where we take $q_{\|}^{p} \alpha\, n_e \times T_e^{1.5}$. Thus, in a magnetically balanced case, we expect a heat flux asymmetry to be biased toward the LO divertor in comparison with the UO divertor. With the same set or arguments, the higher density and lower T_e at the LI target (compared with the UI target) also leads to lower heat flux at the LI target (compared with the UI target). Preliminary UEDGE modeling of a DIII–D-like DN discharge [12] qualitatively supports this interpretation.

Out/in asymmetries in DN: The same set of arguments can be applied to in/out asymmetry. The higher density and lower T_e at the LI target (compared with the UI target) also leads to lower heat flux at the LI target (compared with the UI target). With the result in the above paragraph, we would expect the out/in ratio to be higher in the lower divertor than in the upper divertor (as observed). Based only on "geometric" arguments, we would expect some out/in peak heat flux asymmetries in both upper and lower divertors for balanced DNs. First, the radial gradients of density and temperature on the low field (outboard) side are about twice those of the high field (inboard) side. Second, the ratio of plasma surface area outboard of the separatrices to the area inboard of the separatrices is approximately 1.7 for the configurations considered in this study. If we assume that the diffusivities are poloidally uniform and we then relate q_{out}^{p} and q_{in}^{p} $\alpha\ \chi \cdot \nabla_r T \cdot \mathrm{Area}$, we estimate the in/out heat flux ratio ≈ 3–4. This estimate is somewhat less than the measured ratios (i.e. $q_{out}^{p}/q_{in}^{p} \approx 8–20$).

Cooling from radiated power along the inboard and outboard divertor legs could account for some of the discrepancy between measured and predicted out/in heat flux ratio. (Radiated power measurements to the required accuracy were not available during these experiments for quantitative analysis.) A second possibility that could increase the out/in heat flux asymmetry is turbulent transport on the weak field side of the core plasma [13,14]. "Poor" curvature on the outboard side of the X–points and "good" curvature on the inboard side can enhance the power flow losses through the weak field side. For DNs, this "enhanced" power loss on the weak field side is directed into the outboard divertors and is cutoff from the inboard divertors. Divertor heating on the inboard side must then rely on the less lossy transport on the strong field side. Thus, this "severing" of the inboard and outboard transport in DNs could enhance q_{out}^{p}/q_{in}^{p} over the simple geometric predictions discussed above. While this interpretation is still at the hypothesis stage, reflectometer fluctuation measurements of the outboard midplane made during this experiment gives some support to it, i.e., an increase in density fluctuation amplitude, as the plasma goes from an unbalanced to magnetic configuration (and conversely, a decrease in fluctuation amplitude in going from balanced to unbalanced configuration).

5. SUMMARY AND CONCLUSIONS

We have shown that the peak heat flux balance (up/down and in/out) is highly sensitive to variation in magnetic balance near the double-null configuration in attached plasmas, and this sensitivity is characterized by the scrape off width of the parallel heat flux at the outboard midplane $\lambda_{q_{||}}$. Our data is consistent with E×B poloidal drift playing an important role in these observed asymmetries. The strong in/out heat flux asymmetries for DNs may relax the cooling requirements for handling the power flowing to the inboard divertors sufficiently to make active cooling of the inboard divertors and simplify the engineering of the inboard divertor. This reduced cooling need would be an advantageous feature for high triangularity, low aspect ratio tokamaks. Particle flux to the outboard divertors is less sensitive to changes in magnetic balance. This implies that magnetic balance control may be less critical to particle pumping. Degradation of τ_E with gas injection was seen for all values of drSEP.

REFERENCES

[1] T.D. Rognlien, *et al.*, J. Nucl. Mater., **266-269** (1999) 654.

[2] T.W. Petrie, *et al*, Nucl. Fusion **37** (1997) 321.

[3] L.L. Lao, *et. al.*, Nucl. Fusion **25** (1985) 1611.

[4] C.J. Lasnier, *et. al.*, Nucl. Fusion **38** (1998) 1225.

[5] P.N. Yushmanov, *et al.*, Nucl. Fusion **30** (1990) 1999.

[6] R.J. Groebner and T.H. Osborne, Phys. Plasmas **5** (1998) 1800.

[7] W.W. Pfeiffer, “ONETWO:A Computer Code For Modeling Plasma Transport in Tokamaks,” General Atomics Report GA-A16178 (1980).

[8] W.M. Stacey, Phys. Plasmas **6** (1999] 2452.

[9] W. M. Stacey, T.W. Petrie, (submitted to Phys. Plasmas, 2000).

[10] J.A. Boedo, *et al.*, Phys. Plasmas, **7** (2000) 1075.

[11] T.D. Rognlien, *et al.*, Plasma Phys. **34** (1994) 362.

[12] M. Rensink, (private communication).

[13] G.R. Tynan, “On the Origins of Tokamak Edge Turbulence and the H–mode Transition,” Advanced Series in Nonlinear Dynamics, Vol. 9, World Scientific Pub., (1995) 254.

[14] X. Xu, *et al.*, 13th U.S. Transport Task Force (TTF) Workshop, Burlington, Vermont, April 26-29, 2000.

ACKNOWLEDGMENT

Work supported by the U.S. Department of Energy under Contract Nos. DE-AC03-99ER54463, W-7405-ENG-48, DE-AC04-94AL85000, and Grant No. DE-FG03-86ER53225.